Calin-Vasile PRODAN, Iacob-Liviu SCURTU

AERODYNAMICS STUDY OF THE SOCCER BALL

Abstract: *From the oldest times football, it has become a social phenomenon, being the most famous sport on the planet. Currently in the develop of football infrastructure is necessary to include related and direct activities such as: soccer coach, mass-media, stadium building, etc. Technological progress had also imposed itself on this game area, researching of the new materials and the manufacturing methods for the soccer ball. In this paper is presented the comparative aerodynamic CFD study of three types of ball: smooth sphere ball, Tsubasa and Pelada ball at three air velocity cases. In first part of the paper are presented the state of the art regarding the ball aerodynamics. The second part highlight the forces that act on the ball surface when it is shot by the player and the mathematical k-ε standard turbulence model applied in this study. In the third part are establish the airflow regime by calculating the Reynolds number for each velocity case and the boundary conditions and the CFD simulation are done. The results are presented in the fourth part of the paper, comparing the obtained values for each simulation case. The conclusions and discussion regarding this study are presented in the last part of the paper.*

Key words: *ball aerodynamics, CFD simulation, drag coefficient, airflow regime.*

1. INTRODUCTION

Nowadays, the football is one of the most popular sports in the world due to the large number of practitioners and the clear and easy rules of this sport. The football game has the origin and traditions from the older time, highlighting that the football was played in different country, would be Ancient China, Egypt, and Rome. One very important thing is that in the beginning football was not as we know it today.

Over time, this sport, also called “king sport”, has undergone several important rules transformations. With a tradition of about 2000 years, at the beginning football did not have a set of clear play rules, so each team played as it considered, which made practicing it very difficult, thus introducing the general and the valid rules was necessary so that competitions would take place in the best conditions.

Meantime, the sports competitions have appeared at amateur level and then at professional level, from competitions in international championships to tournaments and world championships, creating a personalized ball for each type of competition.

The technological progress is constantly growing, which has eventually led to the achievement of football balls that fulfil the highest standards. In the last time the ball manufacturers have introduced new models, these are visible in many competitions, but these has a limited data regarding the aerodynamic behaviour of the ball. If in 1970 a football ball had 32 sewn leather panels – 12 pentagonal and 20 hexagonal panels, today we can say that the same ball has in its construction 8 curved synthetic (PVC) thermally bonded panels, or in some cases only 4 synthetic panels. Thermal bonding removes the panel sewing method thus obtaining a more uniform, smoother surface and the ball has a lower weight.

The main objective of this paper is to evaluate the aerodynamic properties of a football ball using the numerical simulation method. The aerodynamic study performed in this paper are applied on three types of balls all having the same size, but different textured profile on their outer surface.

It has been taken into consideration the fact that the Reynolds number will have different values depending on the flow regime (laminar or turbulent) and it is very important if the surface of the ball is smooth or rough. If the ball has seams, then they produce a certain surface roughness determining a different value of the Reynolds number. It is also important if the ball rotates in the air or not.

There are very applied studies of other researchers that have highlighted important results on the aerodynamics of football balls, therefore we can mention results of research conducted by T. Asai et al., 2007, Alam Harun et al., 2021, and others [1], [3]. Many studies were conducted on various football balls having different outer surfaces and different ball manufacturing technologies. The rougher of the outer surface of ball, can have an influence on the aerodynamic performance of the football [2].

In this paper using the CFD evaluation method two football models are evaluated in comparison with a sphere of the same dimensions as a football.

2. MATHEMATICAL APPROACH

2.1 Aerodynamic forces

The aerodynamic forces that act on the ball surface are calculated to establish the aerodynamic performance of the soccer ball.

Using the CFD simulation, in this study are calculated the values of the drag force, lift force and side force. In relation 1 is presented expression of the drag force, that act in the opposite wind direction. The lift force presented in relation 2, act perpendicular to wind direction [1], [4]. The force that acts from lateral side based on a front view is called side force. The expression of this force is presented in relation 3.

$$F_x = \frac{1}{2} \cdot \rho \cdot V^2 \cdot C_D \cdot A \quad (1)$$

where: F_x - drag force, ρ - air density, V - airflow velocity, C_D - drag coefficient, A - cross-sectional area of the ball.

$$F_z = \frac{1}{2} \cdot \rho \cdot V^2 \cdot C_L \cdot A \quad (2)$$

where: C_L - lift coefficient.

$$F_y = \frac{1}{2} \cdot \rho \cdot V^2 \cdot C_S \cdot A \quad (3)$$

where: C_S - side coefficient.

The computed aerodynamic forces are converted to the drag coefficient, lift coefficient and side coefficient, as shown in relation 4, 5, 6:

$$C_D = \frac{2 \cdot F_x}{\rho \cdot V^2 \cdot A} \quad (4)$$

$$C_L = \frac{2 \cdot F_z}{\rho \cdot V^2 \cdot A} \quad (5)$$

$$C_y = \frac{2 \cdot F_y}{\rho \cdot V^2 \cdot A} \quad (6)$$

2.2 Reynolds number

The Reynolds number represent a dimensionless value that establish the relation between the inertial forces and viscous force of a fluid in motion. The value of this number may predict the flow regime and its determination represent the first step to perform an aerodynamic analysis [5]. In relation 7 the expression of the Reynolds number is presented:

$$R_e = \frac{\rho \cdot V \cdot L}{\mu} \quad (7)$$

where: ρ - air density, V - airflow velocity, L - length of the model (ball diameter), μ- dynamic air viscosity.

To determine the flow around the ball model, the Reynolds number value is calculated for six velocity cases: 1, 3, 5, 10, 30 and 50 m/s. These velocity cases have been chosen because the ball velocity varies in the range of 0-50 m/s. The speed record has been reached by Ronny Heberson, with a ball speed of 58.6 m/s (211 km/h) [8].

Table 1

Reynolds number results

Air velocity [m/s]	1	3	5
R_e	1.56E+04	4.69E+04	7.82E+04
Air velocity [m/s]	10	30	50
R_e	1.56E+05	4.69E+05	7.82E+05

This study was performed at a temperature of 15 °C, corresponding the air density ρ=1.225 kg/m^3, the dynamic air viscosity μ= 1.802 · 10^{-5} kg/m·s and the ball diameter L=0.23 mm.

In table 1, the resulted Reynolds number are presented. It can be observed that the flow regime is situated in range of 10^3-10^5, resulting a turbulent flow rate.

3. CAD MODELLING

In this section two soccer ball are modelled: Tsubasa and Pelada ball. The balls CAD model are made by SolidWorks software using advantages modelling techniques. Both balls have modelled at 230 mm diameter. Following, in this paragraph are presented the basic modality to balls models creation [6], [7].

3.1 Tsubasa ball

The Tsubasa ball is the name of the official match ball of FIFA Cluj World Cup 2019. First step to create the ball model is represented by the developed outer profile, presented in Figure 1.

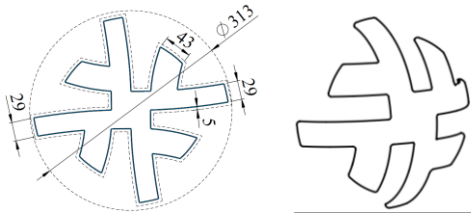

Figure 1 Tsubasa ball profile.

The resulted panel profile is assembled into the final ball model using the assembly module. The ball assembly has built from same six panels, presented in Figure 2.

Figure 2 Tsubasa ball assembly.

3.2 Pelada ball

The second soccer ball modelled is Pelada 2020, made up of 20 hexagonal and 12 pentagonal panels [9]. The shape and the side length of the panels are presented in Figure 3.

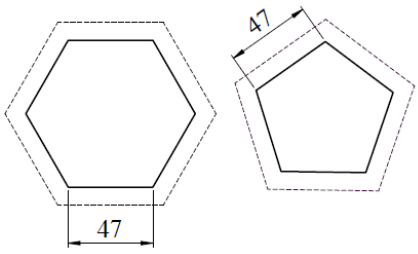

Figure 3 Pelada elements shape.

To create the Pelada ball, each hexagon and pentagon are assembled according to figure 4 where can be seen the assembly modality to create the final model.

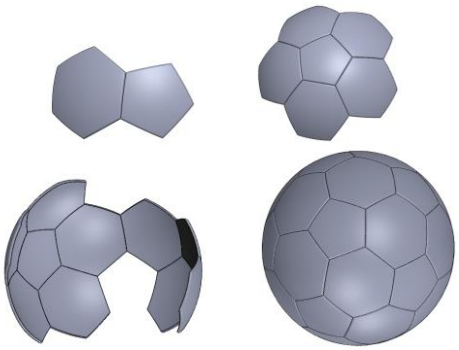

Figure 4 Assembling modality of the Pelada ball model.

4. CFD SIMULATION

In this section, the CFD simulation steps are presented for three soccer ball models. All simulations are performed by using the FlowWorks solver from SolidWorks software.

4.1 Computational domain and boundary conditions

The ball is immersed into a computational domain defined by a cube of 1500 mm side, presented in Figure 5.

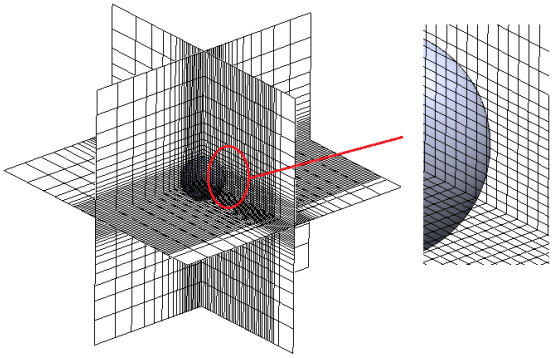

Figure 5 Computational domain discretization.

The computational domain is meshed into 119740 fluid cells, of which 1856 cells are in contact to the sphere contact. To shorten the running time, maintaining the high accuracy results the mesh layers situated near sphere surface are denser, respectively the elements number is higher, as can be seen in figure 5. Even though the Reynolds number was determinate for six ball velocity, the CFD simulation to determinate the drag coefficient is performed for the last three velocity cases. This has been established because the first three velocity cases of the ball are very low to accurately determinate of the drag coefficient.

4.2 Simulation results

In this section are presented the results for all simulation cases. To a better view of the airflow around the ball surface the ball model is represented in an orthogonal and isometric view.

4.3 Sphere results

The first simulation results at 10 m/s are presented in Figure 6. The obtained value of the Reynolds number shows that the airflow regime shows the transition from moderate to turbulent.

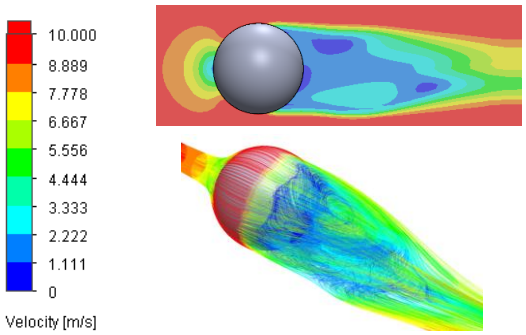

Figure 6 Distribution of the airflow velocity around a sphere at 10 m/s.

It can be observed the viscous flow effect inside of the boundary layer region. In Figure 7 is presented the air pressure distribution around sphere at 10/s, can be observed that the increasing the aerodynamic pressure, the fluid can no longer stick to the sphere surface.

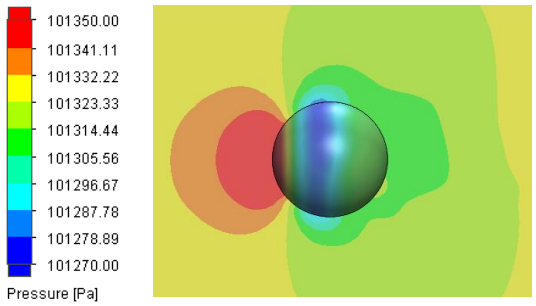

Figure 7 Pressure distribution around a sphere at 10 m/s airflow velocity.

At 30 m/s the boundary layers become thinner in front of the sphere and the flow is unsteady and turbulent behind the sphere.

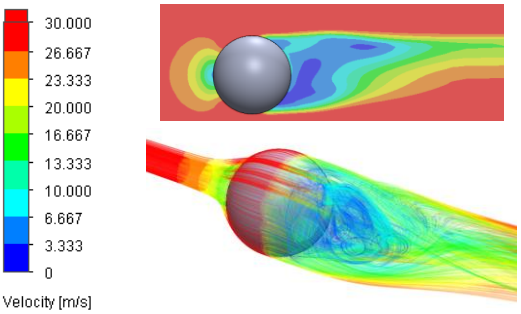

Figure 8 Distribution of the airflow velocity around a sphere at 30 m/s.

The pressure distribution presented in Figure 9 shows that the pressure is lower on the large sphere diameter and the maxim pressure is concentrated on the frontal surface and after the volume region whit low pressure.

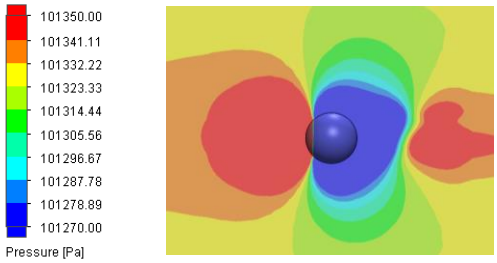

Figure 9 Pressure distribution around a sphere at 30 m/s airflow velocity.

The last velocity case at 50 m/s present a turbulent boundary layer flow, the separation point is situated farther back along sphere, as can be viewed in Figure 10.

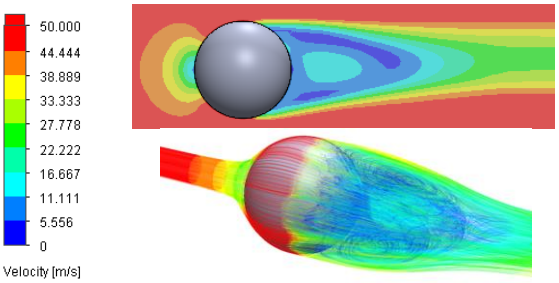

Figure 10 Distribution of the airflow velocity around a sphere at 50 m/s.

Pressure distribution on the sphere surface is concentrated on the air inlet side about 25% of the surface, as can be seen in Figure 11.

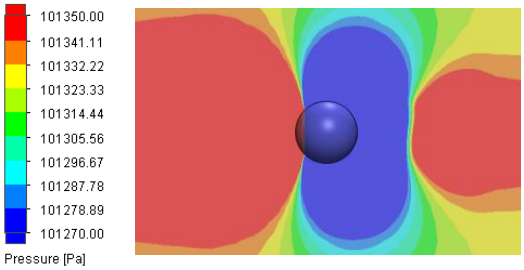

Figure 11 Pressure distribution around a sphere at 50 m/s airflow velocity.

4.4 Tsubasa ball results

In this section are presented the results obtained to second ball model.

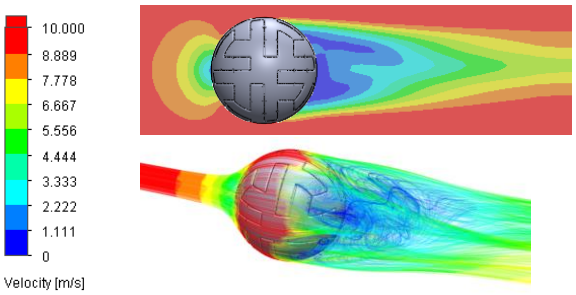

Figure 12 Distribution of the airflow velocity around a Tsubasa ball at 10 m/s.

Compared to the airflow distribution of the smooth sphere case, in this model can be observed in Figure 12, that the groove between the assembled profile allows a smoother airflow behind the ball model. The lower pressure on the ball surface is situated further back, close to the maximum ball diameter, compared to visual results obtained at sphere model, as can be seen in Figure 13.

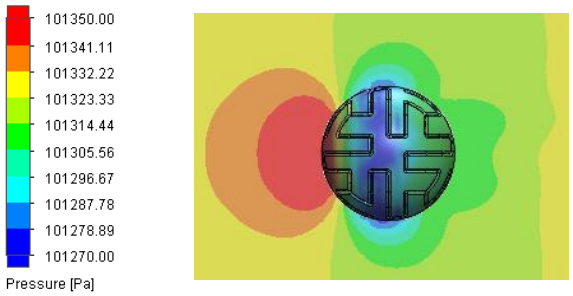

Figure 13 Pressure distribution around a Tsubasa ball at 10 m/s airflow velocity.

Increasing the velocity at 30 m/s shows that the low velocity field is behind of the ball, close to its surface. Comparing with the previous simulation result it can be observed that the low velocity field is smaller, as can be seen in Figure 14**.**

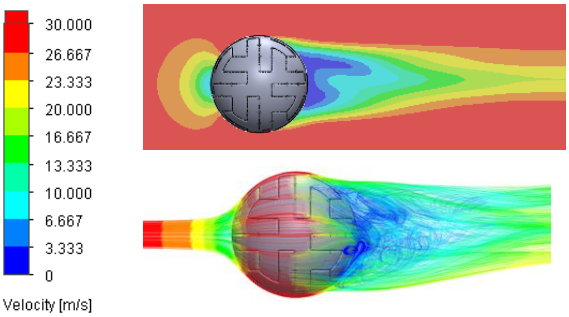

Figure 14 Distribution of the airflow velocity around a Tsubasa ball at 30 m/s.

The air pressure distribution on the ball surface is presented in Figure 15, where it can be seen that the maximum pressure fields appear in the front of ball surface and isolated in rear side after the ball and the low-pressure field.

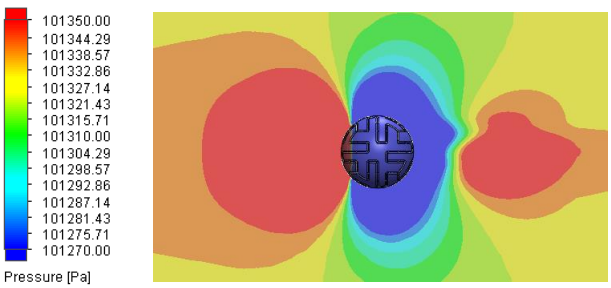

Figure 15 Pressure distribution around a Tsubasa ball at 30 m/s airflow velocity.

In the last simulation case at 50 m/s the air flow tends to become symmetrical in the back side of the ball. The

low velocity field are divided in three area, as can be observed in Figure 16.

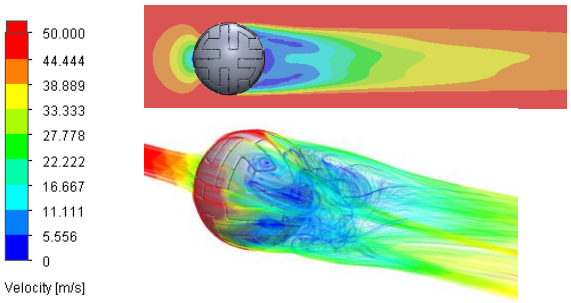

Figure 16 Distribution of the airflow velocity around a Tsubasa ball at 50 m/s.

The high-pressure fields are situated in the front of the ball and applied almost 25% of ball surface and in the rear side of the ball after the low velocity field, presented in Figure 17.

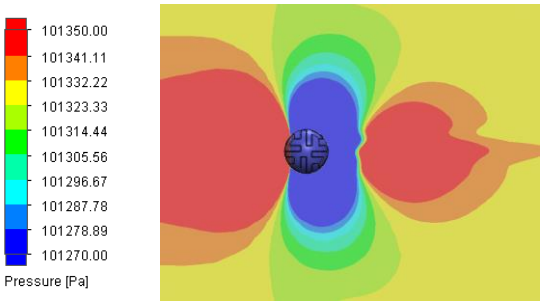

Figure 17 Pressure distribution around a Tsubasa ball at 50 m/s airflow velocity.

4.5 Pelada ball results

The low velocity field resulted at 10 m/s at Pelada ball is smaller and sharper than the results of the previous resulted fields. A better view of the resulted low velocity field is observed in axonometric representation, where can be viewed the separation tendency of the low velocity field, Figure 18.

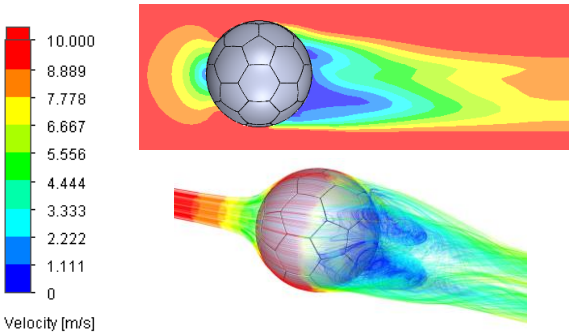

Figure 18 Distribution of the airflow velocity around a Pelada ball at 10 m/s.

The high height air pressure is concentrated on the front side of the ball and the low-pressure field on the ball surface is situated almost on the middle ball surface, as be seen in figure 19.

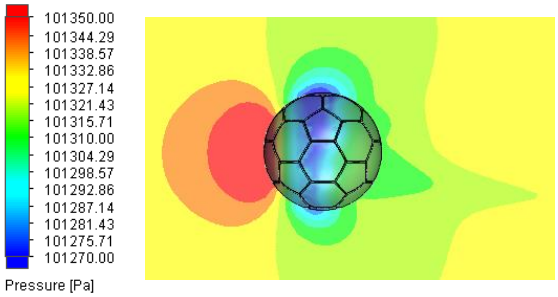

Figure 19 Pressure distribution around a Pelada ball at 10 m/s airflow velocity.

The results at 30 m/s, presented in Figure 20 are like 10 m/s results, but are better visible.

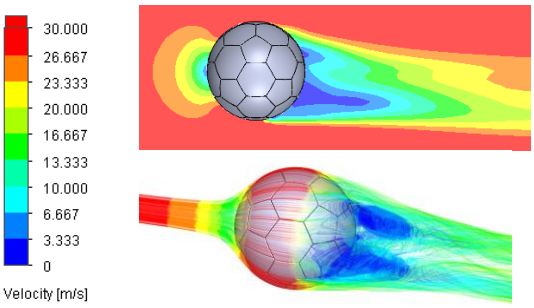

Figure 20 Distribution of the airflow velocity around a Pelada ball at 30 m/s.

The first high air pressure zone is situated on the air inlet side approximate at 30% from ball surface and the second zone is generated after low pressure field on rear side of the ball, as can be seen in Figure 21.

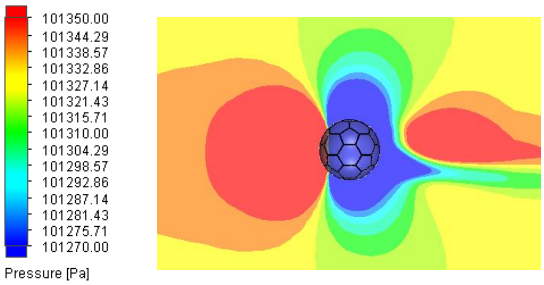

Figure 21 Pressure distribution around a Pelada ball at 30 m/s airflow velocity.

In Figure 22 is presented the velocity of the airflow around the ball geometry. It can be observed that the low velocity field is in the rear ball geometry and are smaller than previous simulation.

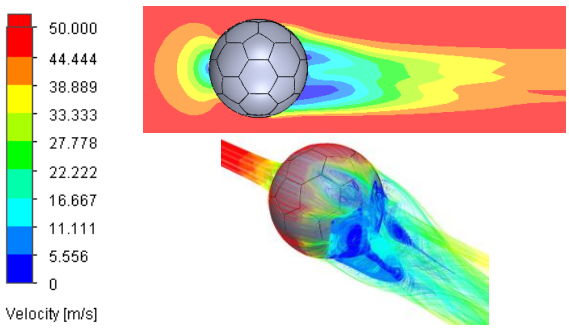

Figure 22 Distribution of the airflow velocity around a Pelada ball at 50 m/s.

In the Figure 23, is presented the air pressure distribution on the ball surface at 50 m/s velocity.

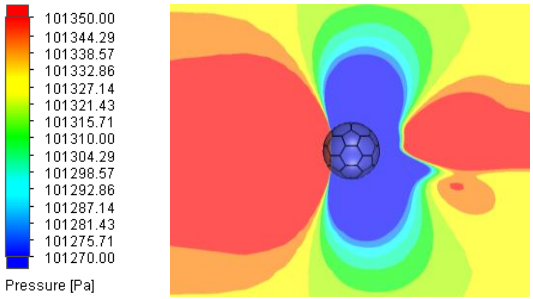

Figure 23 Pressure distribution around a Pelada ball at 50 m/s airflow velocity.

In addition to analysis of the graphical results presented above, the aerodynamic forces and aerodynamic coefficients all calculated for each ball simulation model. In the table 2 is presented the values calculated at 10 m/s air velocity.

Table 2

CFD evaluation results at 10 m/s.

	Sphere	Tsubasa ball	Pelada ball
Drag force [N]	0.606	0.740	0.687
Lift force [N]	0.001	0.089	0.310
Side force [N]	0.001	0.219	0.346
Drag coefficient	0.238	0.291	0.270
Lift coefficient	0.001	0.035	0.122
Side coefficient	0.001	0.086	0.136

In first simulation case at 10 m/s it can be observed that the lift and side force can be neglected because have very low values. The best obtained values are obtained at spheres simulation.

Table 3

CFD evaluation results at 30 m/s.

	Sphere	Tsubasa ball	Pelada ball
Drag force [N]	5.339	6.557	5.992
Lift force [N]	0.185	1.196	3.232
Side force [N]	0.330	2.076	2.694
Drag coefficient	0.233	0.286	0.261
Lift coefficient	0.185	0.052	0.141
Side coefficient	0.014	0.090	0.117

The evaluation results at 30 m/s are presented in table 3. In comparison, the Pelada ball has better aerodynamic performance than Tsubasa ball.

Table 4

CFD evaluation results 50 m/s.

	Sphere	Tsubasa ball	Pelada ball
Drag force [N]	14.403	20.405	16.833
Lift force [N]	3.559	2.507	7.648
Side force [N]	1.188	5.966	7.162
Drag coefficient	0.226	0.320	0.265
Lift coefficient	0.055	0.039	0.120
Side coefficient	0.018	0.093	0.113

At 50 m/s airflow velocity the lower drag coefficient is 0.226 at sphere simulation, as can be seen in table 4.

5. CONCLUSIONS

The present study used a CFD simulation to determine the aerodynamics coefficients and aerodynamic forces that acts on the football surface. The advantage of using the CFD simulation is the possibility to proposal an optimal football shape. A drawback of this work is represented by the modality to performing the simulations cases, in the software the ball is fixed, and the air is moving, while the ball is moving, and the air is fixed. In the most cases when the ball is hit by the player, it rotates around its his axis, appearing the Magnus effect. Another aspect is given by the air temperature and humidity variations comparing to the real environment temperature of the CFD domain. This study is solved without applying this effect. Comparing the obtained results, the Pelada ball have a better aerodynamic performance than Tsubasa ball.

REFERENCES

[1] Asai, T., Hong, S. (2021). *Aerodynamics of the newly approved football for the English Premier League 2020–21 season*. Sci Rep 11, 9578 https://doi.org/10.1038/s41598-021-89162-y

[2] Alam, F., Chowdhury, H., Stemmer, M., Wang, Z., & Yang, J. (2012). *Effects of surface structure on soccer ball aerodynamics*. Procedia Engineering, 34, pp 146-151.

[3] Asai, T., Seo, K., Kobayashi, O., & Sakashita, R. (2007). *Fundamental aerodynamics of the soccer ball*. Sports Engineering, 10(2), pp 101-109.

[4] Balcau, M. (2021). *Aerodynamic study of a car towing a motorcycle trailer*. Journal of Automotive Engineering, ISSN 2457 – 5275, Vol. 27-1, pp 31-38.

[5] Jurco, A. N. (2021). *Study of the influence of roof luggage box on a vehicle aerodynamics*. Journal of Automotive Engineering, ISSN 2457 – 5275, Vol. 27-22, pp 15-22.

[6] Kiraly, A. (2019). *Optimizing the forms and dimensions of a field cultivator working knives*. Journal of Industrial Design and Engineering Graphics, 14(1), pp 71-74, Online ISSN 2344-4681.

[7] Kiraly, A., (2002). *Grafica Inginerească*, Editura U.T. PRESS, ISBN 973-8335-35-3, Cluj-Napoca.

[8] https://www.sportbible.com/football/news-the-fastest-shot-in-football-history-reached-a-ridiculous-137-mph-20201130. *Accessed*: 21.02.2022.

[9] https://www.dimensions.com/element/soccer-ball-football-size-5. *Accessed*: 10.03.2022.

Authors:

Asist. Prof. PhD. Eng. Calin-Vasile PRODAN, Technical University of Cluj-Napoca, Faculty of Automotive, Mechatronics and Mechanical Engineering, Department of Automotive Engineering and Transports, E-mail: calin.prodan@auto.utcluj.ro

Lecturer PhD. Eng. Iacob-Liviu SCURTU, Technical University of Cluj-Napoca, Faculty of Automotive, Mechatronics and Mechanical Engineering, Department of Automotive Engineering and Transports, E-mail: liviu.scurtu@auto.utcluj.ro